

# A Mutual Bootstrapping Model for Automated Skin Lesion Segmentation and Classification

Yutong Xie, Jianpeng Zhang, Yong Xia, and Chunhua Shen.

**Abstract**—Automated skin lesion segmentation and classification are two most essential and related tasks in the computer-aided diagnosis of skin cancer. Despite their prevalence, deep learning models are usually designed for only one task, ignoring the potential benefits in jointly performing both tasks. In this paper, we propose the mutual bootstrapping deep convolutional neural networks (MB-DCNN) model for simultaneous skin lesion segmentation and classification. This model consists of a coarse segmentation network (coarse-SN), a mask-guided classification network (mask-CN), and an enhanced segmentation network (enhanced-SN). On one hand, the coarse-SN generates coarse lesion masks that provide a prior bootstrapping for mask-CN to help it locate and classify skin lesions accurately. On the other hand, the lesion localization maps produced by mask-CN are then fed into enhancedSN, aiming to transfer the localization information learned by mask-CN to enhanced-SN for accurate lesion segmentation. In this way, both segmentation and classification networks mutually transfer knowledge between each other and facilitate each other in a bootstrapping way. Meanwhile, we also design a novel rank loss and jointly use it with the Dice loss in segmentation networks to address the issues caused by class imbalance and hard-easy pixel imbalance. We evaluate the proposed MB-DCNN model on the ISIC-2017 and PH2 datasets, and achieve a Jaccard index of 80.4% and 89.4% in skin lesion segmentation and an average AUC of 93.8% and 97.7% in skin lesion classification, which are superior to the performance of representative state-of-the-art skin lesion segmentation and classification methods. Our results suggest that it is possible to boost the performance of skin lesion segmentation and classification simultaneously via training a unified model to perform both tasks in a mutual bootstrapping way.

**Index Terms**—Skin lesion segmentation, skin lesion classification, deep convolutional neural network, dermoscopy.

## I. INTRODUCTION

**S**KIN cancer is one of the most common malignancies to affect the elderly worldwide [1], [2]. Dermoscopy is one of the essential means to improve the diagnostic performance and reduce skin cancer deaths [3]. Dermoscopic images produced globally are currently analyzed by dermatologists almost entirely through visual inspection, which requires a high degree of skill and concentration, and is time-consuming

This work was supported in part by the National Natural Science Foundation of China under Grants 61771397, in part by the Science and Technology Innovation Committee of Shenzhen Municipality, China, under Grants JCYJ20180306171334997. (Corresponding author: Y. Xia)

Y. Xie, J. Zhang, and Y. Xia are with the National Engineering Laboratory for Integrated Aero-Space-Ground-Ocean Big Data Application Technology, School of Computer Science and Engineering, Northwestern Polytechnical University, Xi'an 710072, China (e-mail: xuyongxie@mail.nwpu.edu.cn; james.zhang@mail.nwpu.edu.cn; yxia@mail.nwpu.edu.cn). C. Shen is with the School of Computer Science, University of Adelaide, SA, Australia (chunhua.shen@adelaide.edu.au). The first two authors' contribution was made partly when visiting The University of Adelaide.

and prone to operator bias. Computer-aided diagnosis (CAD) has been increasingly studied to assist dermatologists in not only bypassing these issues but also improving the accuracy, efficiency and objectivity of the diagnosis.

There are two significant tasks in building a CAD system of skin cancer: skin lesion segmentation and classification [4], [5]. The segmentation task is used to detect the locations and boundaries of lesions, whereas the classification task is used to diagnose the types of them (e.g. melanoma, nevus, seborrheic keratosis, etc.). Both tasks are challenging due to three reasons: (1) the low contrast between each lesion and its surrounding skin tissue results in fuzzy lesion boundaries; (2) the inter-type skin lesions may share visual similarities, and the intra-type lesions may have visual differences; and (3) skin lesions vary significantly in the visual appearance, which may be corrupted by artifacts like hair, blood vessels, and air bubbles.

A mass of automated skin lesion segmentation and classification methods have been proposed in the literature [4]–[29]. Among them, those based on deep convolutional neural networks (DCNNs) have achieved remarkable success [4], [6]–[10], [18]–[23], [28], [29], which are usually designed for either segmentation or classification task. However, skin lesion segmentation and classification are two highly related tasks. The segmentation can help remove distractions from dermoscopic images, and thus is highly beneficial for improving the accuracy of lesion classification, while class-specific diagnostic information can help highlight the lesion regions, and hence contributes to lesion segmentation. Inspired by this, Yu et al. [24] and Diaz et al. [26] incorporated lesion segmentation into the diagnosis process, using the segmentation results to filter the distractions and improve the classification. However, they did not explore the potential contribution of skin lesion classification to the segmentation task.

The benefit of segmentation to classification is obvious, since the segmentation results provide the region of interests (ROIs), in which the discriminative features can be extracted. However, the classification process relies on and produces only the information of image-level class labels. To use such information for image segmentation, we need employ weakly supervised learning (WSL) methods [30]–[34], which usually consist of three successive steps: (1) leveraging a classification model to obtain a localization map of the target, (2) creating proxy pixel-level labels for image-level labeled images based on the localization map, and (3) using proxy pixel-level labels to train a segmentation model. Nevertheless, a classification model focuses only on the class-specific part of an image, which is not necessarily the entire target, particularly in fine-grained type classification. Hence, the localization map

produced by the classification model may contain part-lesion and non-lesion regions and results very likely in less-accurate proxy labels, which provide bad supervision to the segmentation task and thereby lead to unsatisfying segmentation results.

In this paper, we propose the mutual bootstrapping DCNNs (MB-DCNN) model for simultaneous skin lesion segmentation and classification. This model consists of a coarse segmentation network (coarse-SN), a mask-guided classification network (mask-CN), and an enhanced segmentation network (enhanced-SN). Both coarse-SN and enhanced-SN are trained on data with pixel-level labels (i.e. dense annotation), and mask-CN is trained on data with image-level class labels. We first employ the lesion mask generated by coarse-SN to boost the lesion localization and discrimination ability of mask-CN, and then transfer the improved localization ability from mask-CN to enhanced-SN for accurate skin lesion segmentation. In this way, both segmentation and classification tasks mutually benefit each other, and their performance improves together. Meanwhile, we use a weighted Dice-and-rank loss for segmentation networks, in which the Dice loss has good compatibility with class-imbalanced pixels and is beneficial for small lesion segmentation, whereas the newly designed rank loss poses additional constraints on hard pixels and thus addresses the issues caused by fuzzy boundaries and artifacts. We have evaluated the proposed model on the benchmark ISIC-2017 dataset [35] and PH2 dataset [36], and achieved more accurate skin lesion segmentation and classification performance than the state-of-the-art methods.

The contributions of this work are two-fold. First, based on the idea of leveraging the intrinsic correlation existed in segmentation and classification tasks, we propose the MB-DCNN model to perform skin lesion segmentation and classification simultaneously and boost the performance of both tasks. Specifically, we not only transfer the lesion masks generated by coarse-SN to mask-CN to provide it the prior lesion location information and improve its ability to extract discriminative representations for lesion classification, but also transfer the lesion location information refined by mask-CN to enhanced-SN to facilitate lesion segmentation, avoiding the troublesome production and use of proxy pixel labels. Second, we propose a novel rank loss and jointly use it with the Dice loss in segmentation networks to enhance the segmentation compatibility on images with class-imbalance and hard-easy pixel imbalance.

## II. RELATED WORK

Automated skin lesion segmentation and classification have been studied extensively in the literature [4]–[29]. Traditionally, skin lesion segmentation methods mainly include clustering, thresholding, region growing, and active contour models [4], [6]–[13]. Skin lesion classification methods focus mainly on extracting handcrafted features, including the color, texture, border irregularity, and asymmetry descriptors of lesions [5], [14]–[17] and using one or more of these features to train a classifier such as the K-nearest-neighbor [5], back propagation neural network [14], support vector machine [16], linear classifier [17], and logistic regression and product

units [15]. Despite their prevalence, these methods rely heavily on handcrafted features and suffer a lot from less accuracy.

Since DCNNs offer a unified learning-based solution to feature extraction and classification and avoid the troublesome handcrafted feature extraction, recent years have witnessed the widespread and unprecedented use of DCNNs in dermoscopic image analysis [4], [6]–[10], [18]–[29]. Several DCNN-based skin lesion segmentation methods have been published. Bi et al. [7] proposed a multistage segmentation method, in which early stage fully convolutional networks (FCNs) learn appearance and localization features and late stage FCNs learn the subtle characteristics of the lesion boundaries. Yuan et al. [4] developed a 19-layer deep FCN, which was optimized by using the Jaccard distance loss. Li et al. [6] presented a new dense deconvolutional network based on the residual learning. Mirikhraji et al. [10] proposed to encode the star shape prior into the loss function to guarantee a global structure in each segmentation result. Sarkar et al. [9] presented a robust deep encoder-decoder network to improve the accuracy of obtained lesion boundaries. By contrast, more research efforts have been devoted to the classification of skin lesions. Yu et al. [23] aggregated deep features produced by various layers of a residual network using Fisher vector (FV) encoding. Ge et al. [22] reported a multi-modality DCNN that accepts both the clinical and dermoscopic views of a single lesion and is capable of learning single-modality and cross-modality representations, simultaneously. Hagerty et al. [21] combined handcrafted features and the deep features extracted by ResNet50 [37] for the diagnosis of melanoma. Gessert et al. [20] proposed a patch-based attention architecture with the diagnosis-guided weighted loss. Zhang et al. [18], [19] proposed the synergic deep learning (SDL) model that uses dual DCNNs to address the issues of intra-class variation and inter-class similarity. Zhang et al. [29] designed the attention residual learning (ARL) CNN, in which each ARL block jointly uses the residual learning and a novel attention learning mechanism to improve its ability to discriminative representation.

Despite performance improvements, these DCNN-based methods are limited to perform either the segmentation or classification of skin lesions, ignoring the intrinsic correlation between segmentation and classification, which may lead to mutual benefits to both tasks. To address this issue, Yu et al. [24] introduced a two-stage deep learning framework, under which they first separated the lesion from background, and then cropped the segmented regions as the input of a classification network. Diaz et al. [26] further incorporated the extra lesion structure segmentation network into the diagnosis of skin lesions. Both methods utilize the lesion segmentation results to filter the distractions, and thus improve the classification performance. However, they failed to explore the potential benefit of classification results to the lesion segmentation task, which can be achieved by using the WSL strategy.

WSL methods mainly focus on generating high-quality object cues based on image-level labels to supervise the segmentation. Hong et al. [30] proposed a decoupled network for weakly-supervised segmentation, where the class-specific localization cues are transferred from the classification network to the segmentation network. Kolesnikov et

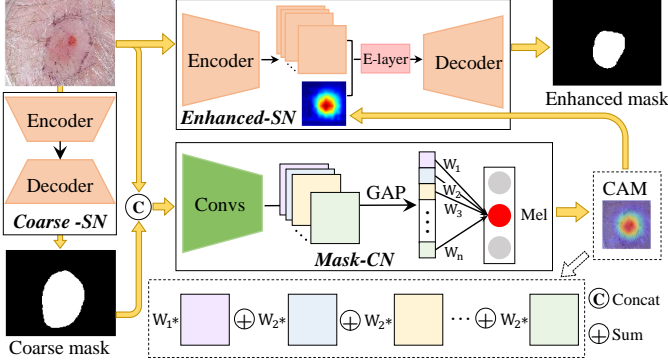


Fig. 1. Illustration of the proposed MB-DCNN model, which consists of three DCNNs: coarse-SN, mask-CN and enhanced-SN. The coarse-SN is constructed to generate the coarse lesion masks, which are concatenated with original images as the input to train mask-CN. The image features extracted by the encoder of enhanced-SN and the lesion localization maps produced by mask-CN are first fused by an E-layer, and then fed into the decoder of enhanced-SN to generate segmentation results.

al. [33] proposed the unified "seed, expand and constrain" (SEC) framework, under which object localization cues, expansion and refining boundary are integrated for segmentation. However, both methods can only provide small and sparse class-related regions to supervise the segmentation, which are not sufficiently accurate for training a reliable segmentation model. To address this drawback, Wei et al. [38] presented an adversarial erasing method to progressively train multiple classification networks for expanding object regions. Shen et al. [32] proposed a bi-directional transfer learning framework to generate high quality object localization masks. Yu et al. [39] and Wei et al. [31] employed the dilated convolutions to enlarge the receptive field and gain more accurate object regions. Although these methods achieve improvements, they only use the classification network to generate localization maps. Different from these attempts, we reveal that a coarse lesion mask can provide a prior bootstrapping to help the classification network better localize and diagnose lesions. Furthermore, both the decoupled network [30] and our model feed the class-related localization maps generated by a classification network to a decoder. However, the decoupled network discards encoder and only trains the decoder, where the error accumulation caused by inaccurate localization can hardly be corrected. Our model fuse image features produced by the encoder and the localization maps as the input of the decoder, and then train the encoder and decoder. Hence, our model can ease the impact of inaccurate localization, which is substantial when using only the localization maps.

### III. METHOD

Let the segmentation training set with  $N_1$  images be denoted by  $I_N = (\mathbf{X}_n, \mathbf{Y}_n)^{N_1}$ , in which each image  $\mathbf{X}_n$  is annotated on a pixel-by-pixel basis and each pixel belongs to either the skin lesion (i.e.  $y_{ni}=1$ ) or background (i.e.  $y_{ni}=0$ ). Let the classification training set with  $N_2$  ( $N_2 > N_1$ ) images be denoted by  $I_M = (\mathbf{X}_m, \mathbf{Y}_m)^{N_2}$ , in which each image  $\mathbf{X}_m$  is annotated with an image-level label  $y_m \in \{l_1, \dots, l_C\}$ , and  $C$  is the number of classes. The proposed MB-DCNN model consists of three DCNNs: coarse-SN, mask-CN, and enhanced-

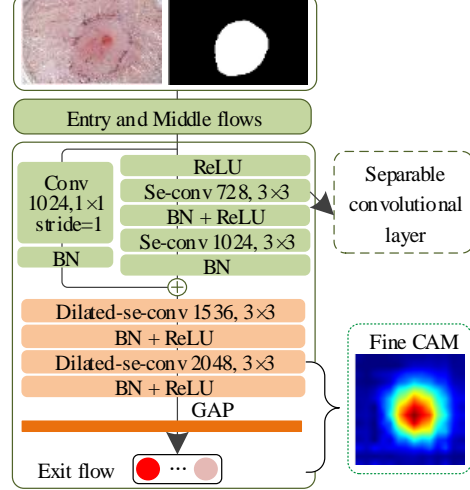


Fig. 2. Architecture of mask-CN, which is built upon the pre-trained Xception [43]. The last pooling layer of Xception is replaced by two dilated convolutional layers with a dilation rate of 2.

SN. The pipeline of this model is summarized in Fig. 1. First, we train coarse-SN on the dataset  $I_N$  for lesion segmentation. Then, we concatenate the images in  $I_M$  with the corresponding lesion masks generated by coarse-SN as the input of mask-CN to boost its performance in lesion classification. Finally, we use an enhanced layer (E-layer) to fuse the features of images in  $I_N$  extracted by the encoder of enhanced-SN and the corresponding lesion localization maps refined by mask-CN, and then feed them to the decoder of enhanced-SN for more accurate lesion segmentation. In this way, both segmentation and classification networks mutually transfer knowledge between each other and boost the performance of each other in a bootstrapping way. We now delve into the details of this model.

#### A. Coarse-SN

We first train coarse-SN using the dataset  $I_N$  to roughly segment skin lesions. The obtained coarse masks provide mask-CN the prior information about lesion locations, and hence can enhance the localization and discrimination ability of mask-CN. This step can be viewed as the initialization of lesion masks. We employ the state-of-the-art semantic segmentation network Deeplabv3+ [40], pre-trained on the MS-COCO [41] and PASCAL VOC 2012 datasets [42], as the backbone of coarse-SN. To adapt the Deeplabv3+ network to our skin lesion segmentation task, we remove its last convolutional layer, and then added a new convolutional layer with the output channel of one for prediction. The weights of the new layer are randomly initialized, and the activation function in the last layer is set to the sigmoid function.

#### B. Mask-CN

We use the coarse lesion masks generated by coarse-SN to boost the lesion localization and discrimination ability of the classification network mask-CN, which is trained on the dataset  $I_M$ , in which each image has only an image-level class label. The region of a skin lesion usually occupies only a small part of a dermoscopic image, and most parts of the image are

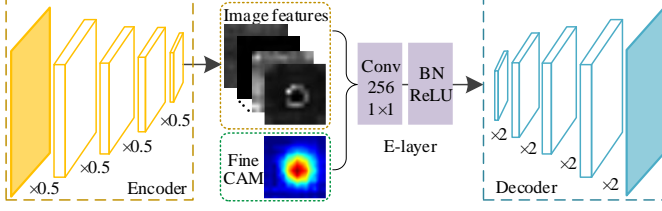


Fig. 3. Architecture of enhanced-SN which consists of an encoder, an E-layer, and a decoder. The encoder and decoder have the same architecture with those in coarse-SN, and the learnable E-layer is designed to fuse image features extracted by the encoder and the fine CAM produced by mask-CN.

normal skin tissues with artifacts such as hair, frames, blood vessels, and air bubbles, which may interfere with the lesion classification. The lesion masks can help remove distractions from dermoscopic images, and thus are highly beneficial for accurate discrimination of lesions.

Each classification training image  $X_m$  and its corresponding coarse lesion mask are concatenated as an input to mask-CN, whose architecture is shown in Fig. 2. This network is built upon the popular classification network Xception [43], which was pre-trained on the ImageNet dataset [44]. We first remove the last pooling layer of Xception to enlarge the resolution of feature maps and avoid the loss of information about small lesions in progressive downsampling. Then, we replace the last two separable convolutions of Xception with the separable dilated convolution with a dilated rate of 2, aiming to compensate for the reduction in receptive field caused by removing downsampling. After performing the global average pooling (GAP), the produced features are fed to a new fully connected (FC) layer with  $C$  neurons, followed by a softmax activation function. The weights of the FC layer are randomly initialized. The weights of the 4th channel (i.e., coarse mask) on input are initialized by averaging the weights of another three channels (i.e., RGB image). We optimize the mask-CN by minimizing the cross-entropy loss.

### C. Enhanced-SN

For each segmentation training image  $X_n$ , we feed it into the trained mask-CN and use the output of the last convolutional layer to produce the class-specific localization maps  $M_n$  via the classification activation mapping (CAM) [45]. Specifically, we first weight the feature maps produced by the last convolutional layer of mask-CN using the class-specific weights of the output layer, and then sum up the weighted feature maps over all channels to generate the class-specific localization maps  $M_n$ . This process is illustrated in Fig. 1.

The architecture of enhanced-SN is shown in Fig. 3, which consists of an encoder, a decoder, and an E-layer between them. The encoder and decoder share the same architecture and parameters with coarse-SN. To incorporate the refined prior information about lesion locations in  $M_n$  into the segmentation process, the E-layer first concatenates the feature maps produced by the encoder with  $M_n$ , and then employs a  $1 \times 1$  convolutional layer followed by a batch normalization (BN) layer and the ReLU activation function for information fusion, i.e. fusing the high-level image features and lesion localization information. The resultant feature maps produced

by the E-layer are fed into the decoder for fine segmentation. We randomly initialize the weights of the E-layer and train the enhanced-SN using pixel-level labels.

### D. Hybrid loss for coarse- and enhanced-SN

To optimize both coarse-SN and enhanced-SN, we propose the following hybrid loss function

$$L_{hybrid} = L_{dice} + \lambda L_{rank} \quad (1)$$

where  $L_{dice}$  is the Dice loss,  $L_{rank}$  is a rank loss, and  $\lambda$  is a weighting factor that balances both loss functions.

The Dice loss measures the degree of agreement between the prediction and ground truth, shown as follows

$$L_{dice} = 1 - \frac{2 \sum_{i=1}^V p_i y_i}{\sum_{i=1}^V (p_i + y_i) + \varepsilon} \quad (2)$$

where  $V$  denotes the number of pixels,  $p_i$  represents the predicted probability of the  $i$ th pixel belonging to the lesion,  $y_i$  represents the ground truth label of the  $i$ th pixel, and  $\varepsilon$  is a smooth factor. It is commonly recognized that the pixels that can be easily recognized, such as those located in internal lesion and background, contribute little to the optimization, whereas hard pixels (e.g., boundary pixels) provide more information for the learning process. Due to the severe imbalance between hard and easy pixels in each image, it is challenging to train the segmentation network and achieve a high-quality score using the Dice loss alone, although the Dice loss has a strong compatibility on the data with class imbalance [46]. To tackle this issue, we employ a rank loss to pose additional constraints on hard and easy pixels.

We design an online rank scheme to select hard pixels dynamically based on the prediction error, which originates from the observation that hard pixels usually produce bigger errors than easy pixels. Specifically, we rank the pixels of the lesion and background, respectively, by their error after the forward propagation of each batch. The top  $K$  pixels with the largest error in lesion or background are selected as hard pixels in this area. Let  $\mathbf{H}_{ni}^0$  and  $\mathbf{H}_{nj}^1$  be prediction values of the  $i$ th hard pixel of background and the  $j$ th hard pixel of lesion for the  $n$ th input image. We calculate the rank loss as follows

$$L_{rank}(\mathbf{X}_n, \mathbf{Y}_n) = \frac{1}{K^2} \sum_{i=1}^K \sum_{j=1}^K \max\{0, \mathbf{H}_{ni}^0(\mathbf{X}_n, \mathbf{Y}_n) - \mathbf{H}_{nj}^1(\mathbf{X}_n, \mathbf{Y}_n) + margin\} \quad (3)$$

which enforces  $\mathbf{H}_{nj}^1 > \mathbf{H}_{ni}^0 + margin$  in the training stage. Such a design enables a segmentation network to pay more attention to those hard pixels and thus learn more discriminative information.

## IV. DATASETS

Three dermoscopic image datasets were used for this study.

**ISIC-2017 dataset.** The 2017 International Skin Imaging Collaboration (ISIC) skin lesion segmentation challenge dataset [47] contains 2000 training, 150 validation, and 600 test dermoscopic images. Each image is paired with the expert manual tracing of skin lesion boundaries for the segmentation

task and the lesion gold standard diagnosis (i.e., melanoma, nevus and seborrheic keratosis) for the classification task.

**ISIC additional dataset.** We collected additional 1320 dermoscopic images from the ISIC archive<sup>1</sup> to expand the training set for the classification task. These images have only image-level labels, including 466 melanoma, 32 seborrheic keratosis, and 822 nevus cases.

**PH2 dataset.** The PH2 public dataset [36] contains 200 dermoscopic images, including 160 nevus, and 40 melanomas. All of them were obtained on the same conditions through Tuebinger Mole Analyzer system using a 20-fold magnification and paired with the expert manual tracing of the skin lesion boundaries.

## V. EXPERIMENTS AND RESULTS

### A. Implementation details

**Training phase.** In the proposed MB-DCNN model, both coarse-SN and enhanced-SN were trained on the ISIC-2017 training dataset using pixel-level labels, and mask-CN was trained on both the ISIC-2017 training dataset and ISIC additional dataset using image-level labels only. To further enlarge the training dataset, we employed the online data augmentation, which includes randomly cropping from the central of each training image with the scale from 50% to 100% of the original image size, random rotation from 0 to 10 degrees, shear from 0 to 0.1 radian, shift from 0 to 20 pixels, zoom 110% of width and height, whitening, horizontal and vertical flips. The augmented patches were then resized to 224224 for training. The Adam algorithm [48] with a batch size of 16 and 32 were adopted to optimize the segmentation and classification networks, respectively. We set the initialized learning rate to 0.0001 and the maximum epoch number to 500, and set the hyper-parameters in the hybrid loss as  $\lambda=0.05$ ,  $K=30$ ,  $margin=0.3$ . We used the ISIC-2017 validation set to monitor the performance of each network and terminated the training process when a network falls into overfitting.

**Testing phase.** On the ISIC-2017 dataset, the trained MB-DCNN was directly applied to the ISIC-2017 testing set for skin lesion segmentation and classification. On the PH2 dataset, we performed two experiments: (1) directly testing the MB-DCNN trained on the ISIC-2017 and ISIC additional datasets (i.e. without fine-tuning) on the entire dataset, and (2) performing the four-fold cross-validation, i.e. regarding the trained MB-DCNN as a pre-trained one, using three folds of PH2 data to fine-tune the model, and testing the fine-tuned model on the other fold of PH2 data. In the second experiment, we also adopted the ISIC-2017 validation set to monitor the fine-tuning process to prevent overfitting.

### B. Evaluation metrics

We evaluated the obtained segmentation results using five performance metrics suggested by the ISIC-2017 challenge, including the Jaccard index (JA), Dice coefficient (DI), pixel-wise accuracy (pixel-AC), pixel-wise sensitivity (pixel-SE), and pixel-wise specificity (pixel-SP). We evaluated the obtained classification results using four performance metrics,

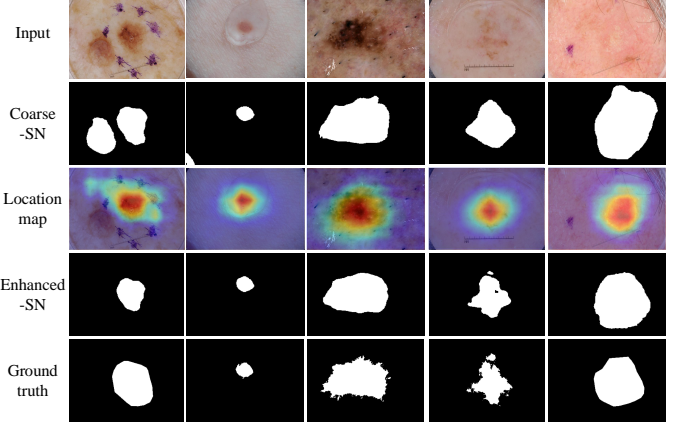


Fig. 4. Examples of predicted lesion masks by our MB-DCNN model. It shows that (1) the coarse-SN can boost mask-CN to produce more accurate localization maps, and (2) the class-specific localization maps are useful to guide enhanced-SN for achieving better segmentation results.

including the area under receive operation curve (AUC), accuracy (AC), sensitivity (SE), and specificity (SP). Note that the ISIC-2017 challenge uses JA to rank the segmentation performance of each method on the test dataset, and uses the average AUC of melanoma classification (i.e. melanoma vs. others) and seborrheic keratosis classification (i.e. seborrheic keratosis vs. others) to rank the classification performance.

### C. Segmentation results

We compared the proposed MB-DCNN model to several recently published skin lesion segmentation methods in Table I. On the ISIC-2017 dataset, the competing methods include a convolutional-deconvolutional neural network (CDNN) [8], a new dense deconvolutional network (DDN) [6], a fully convolutional network with star shape prior (FCN+SSP) [10], and a skin lesion segmentation deep model based on dilated residual and pyramid pooling network (SLSDeep) [9]. On the PH2 dataset, the competing methods consist of multi-stage FCN with parallel integration (mFCNPI) [7], a retrained FCN (RFCN) [4], and a simple linear iterative clustering (SLIC) method [11]. Note that the performance of all competing methods was adopted in the literature for a fair comparison.

It shows in Table I that our MB-DCNN model achieves the best performance on both datasets. On the ISIC-2017 dataset, our model improves JA by 2.2% when comparing to the SLSDeep [9], which performs the second best. On the PH2 dataset, our model improves JA from 84.0%, which was achieved by the mFCNPI [7], to 86.7%, although using the models trained on the ISIC-2017 training set and ISIC additional dataset without fine-tuning. This result proves that our model has a strong generalization ability. Moreover, after fine-tuning the trained models on the PH2 dataset, our model further increases JA to 89.4% and achieves the best DI of 94.2%. We also visualize some segmentation results in Fig. 4.

### D. Classification results

In the meantime, we also compared the proposed MB-DCNN model to several recently published skin lesion classification methods. On the ISIC-2017 dataset, the competing

<sup>1</sup><https://www.isic-archive.com>

TABLE I  
SKIN LESION SEGMENTATION PERFORMANCE OF OUR MB-DCNN AND SEVERAL RECENT METHODS ON THE ISIC-2017 TESTING AND PH2 DATASET.

Datasets	ISIC-2017					PH2				
	CDNN, 2017 [8]	DDN, 2017 [6]	FCN+SSP, 2018 [10]	SLSDeep, 2018 [9]	Ours	mFCNPI, 2017 [7]	RFCN, 2017 [4]	SLIC, 2018 [11]	Ours	Ours (Fine-tuned)
JA	76.5	76.5	77.3	78.2	<b>80.4</b>	84.0	-	-	86.7	<b>89.4</b>
DI	84.9	86.6	85.7	87.8	<b>87.8</b>	90.7	93.8	-	92.6	<b>94.2</b>
pixel-AC	93.4	93.9	93.8	93.6	<b>94.7</b>	94.2	-	90.4	95.8	<b>96.5</b>
pixel-SE	82.5	82.5	85.5	81.6	<b>87.4</b>	94.9	-	91.0	<b>97.9</b>	96.7
pixel-SP	97.5	<b>98.4</b>	97.3	98.3	96.8	94.0	-	89.7	<b>95.1</b>	94.6

TABLE II  
SKIN LESION CLASSIFICATION PERFORMANCE OF OUR MB-DCNN MODEL, THREE RECENT METHODS, AND FIVE TOP-RANKING CHALLENGE SOLUTIONS ON THE ISIC-2017 TESTING SET.

Methods	Melanoma Classification				Keratosis Classification				Average AUC (%)
	AC	SE	SP	AUC	AC	SE	SP	AUC	
<b>Ours</b>	87.8	72.7	91.5	90.3	93.0	84.4	94.5	97.3	<b>93.8</b>
ARL-CNN [29], 2019	85.0	65.8	89.6	87.5	86.8	87.8	86.7	95.8	91.7
SSAC [49], 2019	83.5	55.6	90.3	87.3	91.2	88.9	91.6	95.9	91.6
SDL [19], 2019	88.8	-	-	86.8	92.5	-	-	95.8	91.3
#1 [50]	82.8	73.5	85.1	86.8	80.3	97.8	77.3	95.3	91.1
#2 [51]	82.3	10.3	99.8	85.6	87.5	17.8	99.8	96.5	91.0
#3 [52]	87.2	54.7	95.0	87.4	89.5	35.6	99.0	94.3	90.8
#4 [53]	85.8	42.7	96.3	87.0	91.8	58.9	97.6	92.1	89.6
#5 [54]	83.0	43.6	92.5	83.0	91.7	70.0	99.5	94.2	88.6

TABLE III  
MELANOMA AND NEVUS CLASSIFICATION PERFORMANCE OF OUR MB-DCNN MODEL AND THREE RECENT METHODS ON THE PH2 DATASET.

Methods	AC	SE	SP	AUC
<b>Ours (Fine-tuned)</b>	94.0	95.0	93.8	<b>97.7</b>
<b>Ours</b>	88.5	82.5	90.0	95.6
CICS [55], 2017	-	100.0	88.2	-
MFLF [56], 2015	-	98.0	90.0	-
CCS [57], 2015	-	92.5	76.3	84.3

methods include the advanced semi-supervised adversarial classification (SSAC) model [49], attention residual learning convolutional neural network (ARL-CNN) [29], synergic deep learning (SDL) model [19], and five top-ranking methods on the ISIC-2017 skin lesion classification challenge leaderboard [50]–[54]. On the PH2 dataset, the competing methods are the clinically inspired CAD system (CICS) [55], multi-feature late fusion (MFLF) [56] method, and color constancy system (CCS) [57]. Similarly, we adopted the performance of all those competing methods in the literature.

The results in Table II show that our model achieves the highest average AUC on the ISIC-2017 testing set, not only higher than the top ranking performance on the challenge leaderboard but also 2.1% higher than the average AUC achieved by the ARL-CNN model [29], which, to our knowledge, is the most accurate solution in the literature.

The results in Table III show that applying directly our MB-DCNN model, which was trained on the ISIC-2017 training set and ISIC additional dataset without fine-tuning, to the PH2 dataset achieves a noticeably higher AUC than the CCS system [57] (from 84.3% to 95.6%), which proves again that our model has a strong generalization ability. By further fine-tuning the trained MB-DCNN model on the PH2 dataset, our model achieves the highest AUC of 97.7%, highest AC of

94.0%, highest SP of 93.8%, and a comparable SE of 95.0%.

## VI. DISCUSSIONS

### A. Hybrid loss and its parameter settings

There are two important hyper-parameters in the proposed rank loss, i.e.  $K$  and  $margin$ , which represent the number of selected hard pixels the constraint between easy and hard pixels, respectively. To investigate the impact of their settings on the segmentation, we attempted to set  $K$  to 10, 30, 50, 100, and 150, and set  $margin$  to 0.1, 0.2, 0.3, and 0.4. We plotted the JA values obtained on the ISIC-2017 validation set versus the values of  $K$  and  $margin$  in Fig. 5. It is clear that the proposed MB-DCNN model achieves the highest JA when setting  $K$  is set to 30 and  $margin$  is set to 0.3. Hence, we empirically set  $K$  to 30 and  $margin$  to 0.3 for this study.

In the hybrid loss, the weighting factor  $\lambda$  is a critical parameter, which is used to balance the Dice loss and rank loss. To investigate the setting of this parameter, we fixed the value of  $K$  to 30 and  $margin$  to 0.3, and repeated the skin segmentation experiment with different values of  $\lambda$ , including 0.01, 0.05, 0.1, and 0.5. The JA values obtained on the ISIC-2017 validation set is depicted in Fig. 6. Obviously, the proposed MB-DCNN model achieves the highest JA when  $\lambda$  is set to 0.05. Therefore, we suggest using 0.05 as the default weighting factor in the hybrid loss.

By combining the Dice loss with a rank loss, the proposed hybrid loss takes into account both the data with imbalanced classes and the data with imbalanced hard-easy pixels. To demonstrate the performance gain caused by our hybrid loss, we also attempted to train the proposed model with the Dice loss only. In Table IV, we compared the skin lesion segmentation performance obtained on the ISIC-2017 validation set when using either the Dice loss or the proposed hybrid loss.

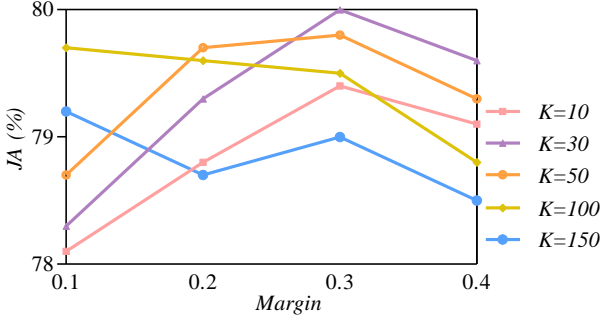


Fig. 5. JA values obtained on the ISIC-2017 validation set versus the values of  $K$  and  $margin$ .

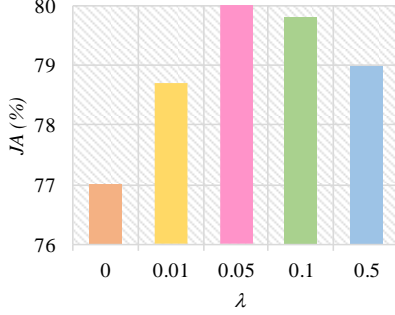


Fig. 6. JA values obtained on the ISIC-2017 validation when the weighting factor  $\lambda$  is set to different values.

It shows that using the hybrid loss to replace the Dice loss improves the value of JA by 3%, i.e. from 77.0% to 80.0%.

### B. Using segmentation to boost classification

In the proposed MB-DCNN model, we concatenate the images and the corresponding lesion masks predicted by coarse-SE as the input of mask-CN, aiming to use the results of skin lesion segmentation to facilitate skin lesion classification. To evaluate the effectiveness of this strategy, we compared the skin lesion classification performance obtained on the ISIC-2017 validation set with or without using the coarse lesion masks produced by coarse-SE in Table V. It reveals that, with the bootstrapping of coarse-SE, our model is substantially more accurate in skin lesion classification, improving the average AUC from 94.9% to 97.0%. Such performance gain is understandable, since the predicted lesion masks enable mask-CN to focus more on lesions instead of background skin tissues on dermoscopic images and thus strengthen the ability of mask-CN to diagnose different lesion types. To further validate this explanation, we visualized three CAMs obtained by mask-CN with or without using the coarse lesion masks in Fig. 7. It shows that, when using the coarse lesion masks, the obtained CAMs are more similar to the segmentation ground truth.

In the proposed MB-DCNN model, we concatenate the images and the corresponding lesion masks predicted by coarse-SE as the input of mask-CN, aiming to use the results of skin lesion segmentation to facilitate skin lesion classification. To evaluate the effectiveness of this strategy, we compared the skin lesion classification performance obtained on the ISIC-2017 validation set with or without using the coarse lesion masks produced by coarse-SE in Table V. It reveals that, with the bootstrapping of coarse-SE, our model is substantially more accurate in skin lesion classification, improving the

TABLE IV  
SKIN LESION SEGMENTATION PERFORMANCE OF OUR MB-DCNN MODEL WITH DIFFERENT LOSS FUNCTIONS ON THE ISIC-2017 VALIDATION SET.

Methods	JA	DI	pixel-AC	pixel-SE	pixel-SP
Dice loss	77.0	84.9	95.4	83.7	<b>95.6</b>
Our hybrid loss	<b>80.0</b>	<b>87.9</b>	<b>96.2</b>	<b>87.4</b>	95.3

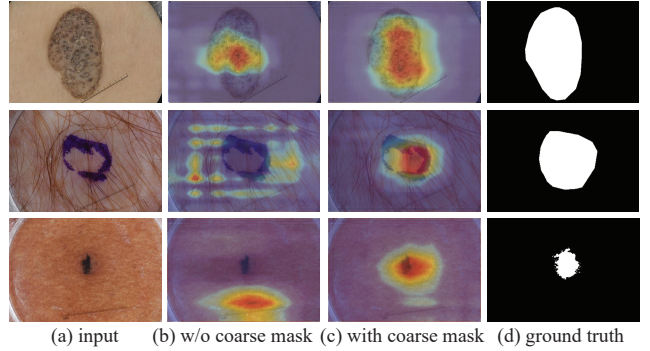


Fig. 7. Comparison of the CAMs obtained by our MB-DCNN model with or without using the coarse lesion masks: (a) three dermoscopic images, (b) CAMs obtained when not using coarse lesion masks, (c) CAMs obtained when using coarse lesion masks, and (d) ground truth for lesion segmentation.

average AUC from 94.9% to 97.0%. Such performance gain is understandable, since the predicted lesion masks enable mask-CN to focus more on lesions instead of background skin tissues on dermoscopic images and thus strengthen the ability of mask-CN to diagnose different lesion types. To further validate this explanation, we visualized three CAMs obtained by mask-CN with or without using the coarse lesion masks in Fig. 7. It shows that, when using the coarse lesion masks, the obtained CAMs are more similar to the segmentation ground truth.

### C. Using classification to boost segmentation

A uniqueness of the proposed MB-DCNN model is to transfer the high-quality lesion localization maps learned by a classification network to a segmentation network to facilitate lesion segmentation. Obviously, the quality of lesion localization maps and the manner of transferring the maps affect the segmentation performance.

**Quality of lesion localization maps.** To assess the impact of the quality of lesion localization maps on the segmentation, we compared the performance of three models on the ISIC-2017 validation set in Table VI. Model A contains only coarse-SE, which does not use any lesion localization maps. Model B contains both mask-CN and enhanced-SE, but without using coarse-SE. As shown in Fig. 7, without the bootstrapping of coarse-SE, the lesion localization maps produced by mask-CN are less accurate. The third model is the proposed one, in which mask-CN provides the high-quality lesion localization maps with the facility of coarse-SE. It shows in Table VI that transferring localization maps from mask-CN without the bootstrapping of coarse-SE to enhanced-SE results in a lower JA than with the bootstrapping (Model B vs. proposed model), even worse than directly using coarse-SE (Model B vs. Model A). The poor segmentation performance is attributed mainly to the fact that the mask-CN without the bootstrapping of coarse-SE has a weak localization ability that damages the performance of enhanced-SE. Our model uses the mask-CN

TABLE V

SKIN LESION CLASSIFICATION PERFORMANCE OF OUR MB-DCNN MODEL WITH OR WITHOUT (W/O) USING THE COARSE LESION MASKS ON THE ISIC-2017 VALIDATION SET.

Methods	Melanoma Classification				Keratosis Classification				Average AUC (%)
	AC	SE	SP	AUC	AC	SE	SP	AUC	
w/o coarse-SN	86.7	63.3	92.5	92.6	94.0	88.1	96.3	97.1	94.9
with coarse-SN	91.3	86.7	92.5	94.6	93.3	100.0	90.7	99.4	<b>97.0</b>

TABLE VI

SKIN LESION SEGMENTATION PERFORMANCE OF THREE MODELS WITH THE LESION LOCALIZATION MAPS OF DIFFERENT QUALITY ON THE ISIC-2017 VALIDATION SET. 'CS' IS COARSE-SN. 'MC' IS MASK-CN. 'ES' IS ENHANCED-SN.

Models	CS	MC	ES	JA	DI	pixel-AC	pixel-SE	pixel-SP
A	✓	✗	✗	78.9	86.5	95.7	88.7	95.0
B	✗	✓	✓	77.7	86.0	95.5	<b>89.1</b>	<b>96.0</b>
<b>Ours</b>	✓	✓	✓	<b>80.0</b>	<b>87.9</b>	<b>96.2</b>	87.4	95.3

TABLE VII

SKIN LESION SEGMENTATION PERFORMANCE OF THREE MODELS WITH DIFFERENT MANNERS OF TRANSFERRING LESION LOCALIZATION MAPS ON THE ISIC-2017 VALIDATION SET.

Methods	JA	DI	pixel-AC	pixel-SE	pixel-SP
D-Net, 2015 [30]	76.2	84.9	94.4	<b>89.5</b>	94.6
MDC, 2018 [31]	78.9	87.0	96.1	86.1	<b>95.9</b>
<b>Ours</b>	<b>80.0</b>	<b>87.9</b>	<b>96.2</b>	87.4	95.3

with the bootstrapping of coarse-SN, and hence can produce high-quality localization maps, which in turn enable enhanced-SN to achieve a better performance than coarse-SN (Proposed model vs. Model A).

**Manner of transferring lesion localization maps.** Besides the quality of lesion localization maps, the manner of transferring the maps from mask-CN to enhanced-SN also matters. The MDC method [31] creates proxy pixel-level labels for the images with only image-level labels based on localization maps, and then trains two segmentation networks by jointly using both real and proxy pixel-level labels. To avoid the impact of inaccurate labels, once localization maps are obtained, the decoupled network (D-Net) [30] and our MB-DCNN model train only one segmentation network, to which the localization maps are transferred. Nevertheless, the D-Net only transfers localization maps to the decoder, and our model, by contrast, fuses the maps with the image features produced by the encoder and feeds them to the decoder. We compare the segmentation performance of these three models in Table VII. For a fair comparison, the MDC method and our model use the same segmentation network, i.e. Deeplabv3+ [40], and the D-Net and our model use the same decoder. It shows that our model is able to ease the error accumulation caused by the inaccurate localization maps, and hence achieves an improvement of 3.8% in JA over the D-Net. The results also suggest that, with the transfer of lesion localization maps, our model improves JA by 1.1% over the MDC method.

#### D. Advantages of mutual bootstrapping

The proposed MB-DCNN model can not only transfer the lesion location produced by a segmentation network to mask-CN to facilitate lesion classification, but also transfer the high-quality lesion localization information learned by mask-CN to

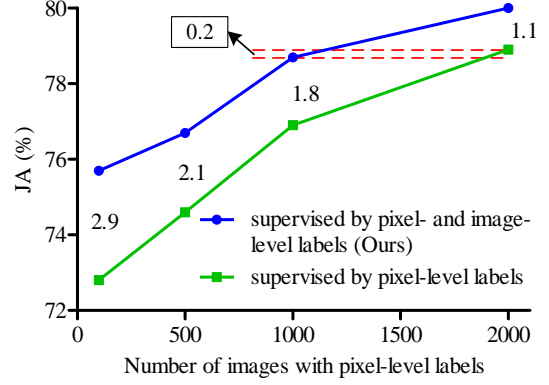


Fig. 8. JA values achieved on the ISIC-2017 validation set by MB-DCNN model (trained on some images with pixel-level labels and some with image-level labels) and a fully-supervised segmentation network (trained only on images with pixel-level labels), when the number of training images with pixel-level labels increases from 100 to 2000.

enhanced-SN to alleviate the impact of inaccurate localization on segmentation results. As a result, both segmentation and classification networks mutually facilitate each other in a bootstrapping way, and thus boost the performance of both skin lesion segmentation and classification simultaneously, particularly when the training set is small.

A major advantage of using classification to boost segmentation is to use the images with only image-level annotations to facilitate the training of a segmentation network, leading to less requirement of the pixel-level dense annotation. To demonstrate this advantage, we compared the proposed MB-DCNN model to a fully-supervised segmentation model, which has the same architecture to enhanced-SN and is trained only on the images with pixel-level labels, but without using any lesion localization maps. The JA values of both solutions on the ISIC-2017 validation set versus the number of training images with pixel-level labels were plotted in Fig. 8. As expected, with the weak supervision provided by image-level labels, our model outperforms the fully-supervised one steadily no matter how many training images with pixel-level labels were used. However, the performance gain reduces from 2.9% to 1.1% when the number of densely annotated training images increases from 100 to 2000. It is not surprising, since the more densely annotated training images are used, the less weakly annotated images are needed for auxiliary training.

More important, it is interesting that the JA achieved by our model trained with 1000 densely annotated images is only 0.2% less than the JA achieved by the fully supervised method trained with 2000 samples. A similar phenomenon can be found when the number of densely annotated training images used by both methods reduces to 500 and 1000, respectively. It suggests that our model provides the possibility of using weakly annotated training images to replace almost

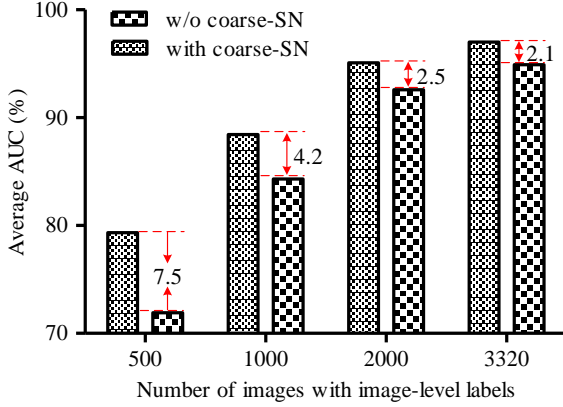


Fig. 9. Average AUC values obtained on the ISIC-2017 validation set by our MB-DCNN model with or without the help of coarse-SN when the number of image-level annotated training images increases from 500 to 3320.

half of densely annotated training images while maintaining the segmentation performance.

By contrast, the advantages of using segmentation to boost classification is quite explicit, since segmentation results provide a classification network the regions of skin lesions, in which discriminative features should be extracted. Although the classification network can generate such regions of interest by itself, using the lesion masks produced by the segmentation network as part of the input results in more accurate regions of interest, as shown in Figure 7, which in turn improve the classification performance. To demonstrate the sustainability of such performance improvement, we kept the validation dataset and pixel-level annotated training set unchanged, and selected randomly 500, 1000, and 2000 image-level annotated images to train our MB-DCNN model with or without the help of coarse-SN, respectively. We compared their average AUC on the ISIC-2017 validation set in Figure 9. As expected, with the help of the lesion masks, our model outperforms the model without coarse-SN steadily, no matter how many image-level annotated training images were used. However, the classification performance gain reduces from 7.5% to 2.1% when the number of training images with image-level labels increases from 500 to 3320. It suggests that the less training data we have, the greater role the lesion masks may play.

Meanwhile, it reveals that, with the help of lesion masks, our model trained on 2000 images has similar performance to the model without using lesion masks but being trained on 3320 images. It indicates that using the lesion masks produced by coarse-SN can largely compensate the loss of classification power caused by reducing the number of training images.

#### E. Complexity

For this study, three DCNNs in our MB-DCNN model are trained using the open source Keras and Tensorflow software packages. In our experiments, it took about 48 hours to train our MB-DCNN model (24 hours for coarse-SN, 12 hours for mask-CN and 12 hours for enhanced-SN) and less than 1 second to apply it to segment and classify each lesion on a server with 4 NVIDIA GTX 1080 Ti GPUs and 512GB Memory. Although time-consuming, training the model can be

done offline. The fast online testing suggests that our model has the potential to be used in a routine clinical workflow.

## VII. CONCLUSION

In this paper, we have proposed the MB-DCNN model for simultaneous skin lesion segmentation and classification, which consists of a classification network, i.e. mask-CN, and two segmentation networks, i.e., coarse-SN and enhanced-SN. The coarse-SN provides prior bootstrapping to mask-CN for accurately localization and diagnosis of skin lesions, and then the localization ability is transferred to enhanced-SN to obtain accurate lesion segmentation. We also design a novel hybrid loss to optimize both segmentation networks. Our results on the ISIC 2017 dataset and PH2 dataset not only demonstrate the effectiveness of mutual bootstrapping for image segmentation methods and classification, but also indicate that the proposed MB-DCNN model outperforms the state-of-the-art skin lesion segmentation methods and classification methods with substantial margins. Although our algorithm is built upon the specific application of skin lesion analysis, the proposed mutual bootstrapping strategy itself is generic and can be applied to other deep learning-based medical image segmentation and classification tasks to improve the performance of both tasks simultaneously.

## REFERENCES

- [1] R. L. Siegel, K. D. Miller, and A. Jemal, "Cancer statistics, 2019," *CA: a cancer journal for clinicians*, vol. 69, no. 1, pp. 7–34, 2019.
- [2] C. M. Balch, J. E. Gershenwald, S.-J. Soong, J. F. Thompson, M. B. Atkins, D. R. Byrd, A. C. Buzaid, A. J. Cochran, D. G. Coit, S. Ding, A. M. Eggermont, K. T. Flaherty, P. A. Gimotty, J. M. Kirkwood, K. M. McMasters, M. C. Mihm, D. L. Morton, M. I. Ross, A. J. Sober, and V. K. Sondak, "Final version of 2009 ajcc melanoma staging and classification," *Journal of Clinical Oncology*, vol. 27, no. 36, pp. 6199–6206, 2009.
- [3] H. Kittler, H. Pehamberger, K. Wolff, and M. Binder, "Diagnostic accuracy of dermoscopy," *The lancet oncology*, vol. 3, no. 3, pp. 159–165, 2002.
- [4] Y. Yuan, M. Chao, and Y. Lo, "Automatic skin lesion segmentation using deep fully convolutional networks with jaccard distance," *IEEE Transactions on Medical Imaging*, vol. 36, no. 9, pp. 1876–1886, Sep. 2017.
- [5] H. Ganster, P. Pinz, R. Rohrer, E. Wildling, M. Binder, and H. Kittler, "Automated melanoma recognition," *IEEE Transactions on Medical Imaging*, vol. 20, no. 3, pp. 233–239, March 2001.
- [6] H. Li, X. He, F. Zhou, Z. Yu, D. Ni, S. Chen, T. Wang, and B. Lei, "Dense deconvolutional network for skin lesion segmentation," *IEEE Journal of Biomedical and Health Informatics*, vol. 23, no. 2, pp. 527–537, March 2019.
- [7] L. Bi, J. Kim, E. Ahn, A. Kumar, M. Fulham, and D. Feng, "Dermoscopic image segmentation via multistage fully convolutional networks," *IEEE Transactions on Biomedical Engineering*, vol. 64, no. 9, pp. 2065–2074, Sep. 2017.
- [8] Y. Yuan and Y. Lo, "Improving dermoscopic image segmentation with enhanced convolutional-deconvolutional networks," *IEEE Journal of Biomedical and Health Informatics*, vol. 23, no. 2, pp. 519–526, March 2019.
- [9] M. M. K. Sarker, H. A. Rashwan, F. Akram, S. F. Banu, A. Saleh, V. K. Singh, F. U. Chowdhury, S. Abdulwahab, S. Romani, P. Radeva *et al.*, "Slsdeep: Skin lesion segmentation based on dilated residual and pyramid pooling networks," in *MICCAI*, 2018, pp. 21–29.
- [10] Z. Mirikhraji and G. Hamarneh, "Star shape prior in fully convolutional networks for skin lesion segmentation," in *MICCAI*, 2018, pp. 737–745.
- [11] D. Patiño, J. Avendaño, and J. W. Branch, "Automatic skin lesion segmentation on dermoscopic images by the means of superpixel merging," in *MICCAI*, 2018, pp. 728–736.

[12] F. Peruch, F. Bogo, M. Bonazza, V. Cappelleri, and E. Peserico, "Simpler, faster, more accurate melanocytic lesion segmentation through meds," *IEEE Transactions on Biomedical Engineering*, vol. 61, no. 2, pp. 557–565, Feb 2014.

[13] E. Ahn, J. Kim, L. Bi, A. Kumar, C. Li, M. Fulham, and D. D. Feng, "Saliency-based lesion segmentation via background detection in dermoscopic images," *IEEE Journal of Biomedical and Health Informatics*, vol. 21, no. 6, pp. 1685–1693, Nov 2017.

[14] F. Xie, H. Fan, Y. Li, Z. Jiang, R. Meng, and A. Bovik, "Melanoma classification on dermoscopy images using a neural network ensemble model," *IEEE Transactions on Medical Imaging*, vol. 36, no. 3, pp. 849–858, March 2017.

[15] A. Sez, J. Sánchez-Monedero, P. A. Gutierrez, and C. Hervs-Martinez, "Machine learning methods for binary and multiclass classification of melanoma thickness from dermoscopic images," *IEEE Transactions on Medical Imaging*, vol. 35, no. 4, pp. 1036–1045, April 2016.

[16] R. Amelard, J. Glaister, A. Wong, and D. A. Clausi, "High-level intuitive features (hlfs) for intuitive skin lesion description," *IEEE Transactions on Biomedical Engineering*, vol. 62, no. 3, March 2015.

[17] K. Shimizu, H. Iyatomi, M. E. Celebi, K. Norton, and M. Tanaka, "Four-class classification of skin lesions with task decomposition strategy," *IEEE Transactions on Biomedical Engineering*, vol. 62, no. 1, pp. 274–283, Jan 2015.

[18] J. Zhang, Y. Xie, Q. Wu, and Y. Xia, "Skin lesion classification in dermoscopy images using synergic deep learning," in *MICCAI*, 2018, pp. 12–20.

[19] J. Zhang, Y. Xie, Q. Wu, and Y. Xia, "Medical image classification using synergic deep learning," *Medical image analysis*, vol. 54, pp. 10–19, 2019.

[20] N. Gessert, T. Sentker, F. Madesta, R. Schmitz, H. Kniep, I. Baltruschat, R. Werner, and A. Schlaefter, "Skin lesion classification using cnns with patch-based attention and diagnosis-guided loss weighting," *IEEE Transactions on Biomedical Engineering*, pp. 1–1, 2019.

[21] J. R. Hagerty, R. J. Stanley, H. A. Almubarak, N. Lama, R. Kasmi, P. Guo, R. J. Drugge, H. S. Rabinovitz, M. Oliviero, and W. V. Stoecker, "Deep learning and handcrafted method fusion: Higher diagnostic accuracy for melanoma dermoscopy images," *IEEE Journal of Biomedical and Health Informatics*, vol. 23, no. 4, pp. 1385–1391, July 2019.

[22] Z. Ge, S. Demyanov, R. Chakravorty, A. Bowling, and R. Garnavi, "Skin disease recognition using deep saliency features and multimodal learning of dermoscopy and clinical images," in *MICCAI*, 2017, pp. 250–258.

[23] Z. Yu, X. Jiang, F. Zhou, J. Qin, D. Ni, S. Chen, B. Lei, and T. Wang, "Melanoma recognition in dermoscopy images via aggregated deep convolutional features," *IEEE Transactions on Biomedical Engineering*, vol. 66, no. 4, pp. 1006–1016, April 2019.

[24] L. Yu, H. Chen, Q. Dou, J. Qin, and P. Heng, "Automated melanoma recognition in dermoscopy images via very deep residual networks," *IEEE Transactions on Medical Imaging*, vol. 36, no. 4, pp. 994–1004, April 2017.

[25] S. Chen, Z. Wang, J. Shi, B. Liu, and N. Yu, "A multi-task framework with feature passing module for skin lesion classification and segmentation," in *IEEE ISBI*, 2018, pp. 1126–1129.

[26] I. Gonzlez-Daz, "Dermaknet: Incorporating the knowledge of dermatologists to convolutional neural networks for skin lesion diagnosis," *IEEE Journal of Biomedical and Health Informatics*, vol. 23, no. 2, pp. 547–559, March 2019.

[27] X. Yang, H. Li, L. Wang, S. Y. Yeo, Y. Su, and Z. Zeng, "Skin lesion analysis by multi-target deep neural networks," in *IEEE EMBC*, 2018, pp. 1263–1266.

[28] Y. Yan, J. Kawahara, and G. Hamarneh, "Melanoma recognition via visual attention," in *IPMI*, 2019, pp. 793–804.

[29] J. Zhang, Y. Xie, Y. Xia, and C. Shen, "Attention residual learning for skin lesion classification," *IEEE Transactions on Medical Imaging*, vol. 38, no. 9, pp. 2092–2103, Sep. 2019.

[30] S. Hong, H. Noh, and B. Han, "Decoupled deep neural network for semi-supervised semantic segmentation," in *NIPS*, 2015, pp. 1495–1503.

[31] Y. Wei, H. Xiao, H. Shi, Z. Jie, J. Feng, and T. S. Huang, "Revisiting dilated convolution: A simple approach for weakly-and semi-supervised semantic segmentation," in *IEEE CVPR*, 2018, pp. 7268–7277.

[32] T. Shen, G. Lin, C. Shen, and I. Reid, "Bootstrapping the performance of weakly supervised semantic segmentation," in *IEEE CVPR*, 2018, pp. 1363–1371.

[33] A. Kolesnikov and C. H. Lampert, "Seed, expand and constrain: Three principles for weakly-supervised image segmentation," in *ECCV*, 2016, pp. 695–711.

[34] Y. Zhou, X. He, L. Huang, L. Liu, F. Zhu, S. Cui, and L. Shao, "Collaborative learning of semi-supervised segmentation and classification for medical images," in *IEEE CVPR*, 2019, pp. 2079–2088.

[35] N. C. Codella, D. Gutman, M. E. Celebi, B. Helba, M. A. Marchetti, S. W. Dusza, A. Kalloo, K. Liopyris, N. Mishra, H. Kittler *et al.*, "Skin lesion analysis toward melanoma detection: A challenge at the 2017 international symposium on biomedical imaging (isbi), hosted by the international skin imaging collaboration (isic)," in *IEEE ISBI*, 2018, pp. 168–172.

[36] T. Mendonça, P. Ferreira, J. Marques, A. Marcjal, and J. Rozeira, "A dermoscopic image database for research and benchmarking," *Presentation in Proceedings of PH*, vol. 2, 2013.

[37] K. He, X. Zhang, S. Ren, and J. Sun, "Deep residual learning for image recognition," in *IEEE CVPR*, 2016, pp. 770–778.

[38] Y. Wei, J. Feng, X. Liang, M.-M. Cheng, Y. Zhao, and S. Yan, "Object region mining with adversarial erasing: A simple classification to semantic segmentation approach," in *IEEE CVPR*, 2017, pp. 1568–1576.

[39] F. Yu, V. Koltun, and T. Funkhouser, "Dilated residual networks," in *IEEE CVPR*, 2017, pp. 472–480.

[40] L.-C. Chen, Y. Zhu, G. Papandreou, F. Schroff, and H. Adam, "Encoder-decoder with atrous separable convolution for semantic image segmentation," in *ECCV*, 2018, pp. 801–818.

[41] T.-Y. Lin, M. Maire, S. Belongie, J. Hays, P. Perona, D. Ramanan, P. Dollár, and C. L. Zitnick, "Microsoft coco: Common objects in context," in *ECCV*, 2014, pp. 740–755.

[42] M. Everingham, L. Van Gool, C. K. Williams, J. Winn, and A. Zisserman, "The pascal visual object classes (voc) challenge," *International journal of computer vision*, vol. 88, no. 2, pp. 303–338, 2010.

[43] F. Chollet, "Xception: Deep learning with depthwise separable convolutions," in *IEEE CVPR*, 2017, pp. 1251–1258.

[44] J. Deng, W. Dong, R. Socher, L.-J. Li, K. Li, and L. Fei-Fei, "Imagenet: A large-scale hierarchical image database," in *IEEE CVPR*, 2009, pp. 248–255.

[45] B. Zhou, A. Khosla, A. Lapedriza, A. Oliva, and A. Torralba, "Learning deep features for discriminative localization," in *IEEE CVPR*, 2016, pp. 2921–2929.

[46] F. Milletari, N. Navab, and S.-A. Ahmadi, "V-net: Fully convolutional neural networks for volumetric medical image segmentation," in *IEEE 3DV*, 2016, pp. 565–571.

[47] N. C. Codella, D. Gutman, M. E. Celebi, B. Helba, M. A. Marchetti, S. W. Dusza, A. Kalloo, K. Liopyris, N. Mishra, H. Kittler *et al.*, "Skin lesion analysis toward melanoma detection: A challenge at the 2017 international symposium on biomedical imaging (isbi), hosted by the international skin imaging collaboration (isic)," in *IEEE ISBI*, 2018, pp. 168–172.

[48] D. P. Kingma and J. Ba, "Adam: A method for stochastic optimization," *arXiv preprint arXiv:1412.6980*, 2014.

[49] Y. Xie, J. Zhang, and Y. Xia, "Semi-supervised adversarial model for benign–malignant lung nodule classification on chest ct," *Medical image analysis*, vol. 57, pp. 237–248, 2019.

[50] K. Matsunaga, A. Hamada, A. Minagawa, and H. Koga, "Image classification of melanoma, nevus and seborrheic keratosis by deep neural network ensemble," *arXiv preprint arXiv:1703.03108*, 2017.

[51] I. G. Díaz, "Incorporating the knowledge of dermatologists to convolutional neural networks for the diagnosis of skin lesions," *arXiv preprint arXiv:1703.01976*, 2017.

[52] A. Menegola, J. Tavares, M. Fornaciali, L. T. Li, S. Avila, and E. Valle, "Recod titans at isic challenge 2017," *arXiv preprint arXiv:1703.04819*, 2017.

[53] L. Bi, J. Kim, E. Ahn, and D. Feng, "Automatic skin lesion analysis using large-scale dermoscopy images and deep residual networks," *arXiv preprint arXiv:1703.04197*, 2017.

[54] X. Yang, Z. Zeng, S. Y. Yeo, C. Tan, H. L. Tey, and Y. Su, "A novel multi-task deep learning model for skin lesion segmentation and classification," *arXiv preprint arXiv:1703.01025*, 2017.

[55] C. Barata, M. E. Celebi, and J. S. Marques, "Development of a clinically oriented system for melanoma diagnosis," *Pattern Recognition*, vol. 69, pp. 270–285, 2017.

[56] C. Barata, M. E. Celebi, and J. S. Marques, "Melanoma detection algorithm based on feature fusion," in *IEEE EMBC*, 2015, pp. 2653–2656.

[57] C. Barata, M. E. Celebi, and J. S. Marques, "Improving dermoscopy image classification using color constancy," *IEEE Journal of Biomedical and Health Informatics*, vol. 19, no. 3, pp. 1146–1152, May 2015.